Investigation of different registration methods for TLS-based deformation analysis of hydroelectric dams — A case study

Nicholas MEYER[1,*], **Tomislav MEDIC**[1], **Ephraim FRIEDLI**[2], **Rico SENTI**[2], and **Andreas WIESER**[1]

[1] *Institute of Geodesy and Photogrammetry, ETH Zurich, Switzerland (<firstname>.<lastname>@geod.baug.ethz.ch)*

[2] *Axpo Power AG, Baden, Switzerland (<firstname>.<lastname>@axpo.com)*

[*] *corresponding author*

Abstract

In this paper, we investigate various registration techniques for Terrestrial Laser Scanning (TLS) in the context of deformation analysis of hydroelectric dams. Accurate spatiotemporal registration of TLS data is particularly challenging in non-urban and mountainous environments due to the scarcity of unobstructed and geometrically well-defined surfaces. This is compounded by the presence of unknown changes over time in potentially large parts of the scanned scenes. These challenges complicate the establishment of suitable correspondences between the scans. Traditional registration methods often struggle under these conditions, leading to point cloud differences that may be misinterpreted and mask the actual deformations. We apply an approach utilizing optical flow, as well as Feature to Feature Supervoxel-based Spatial Smoothing (F2S3), to determine 3D vector fields between corresponding points and robustly estimate the registration parameters from these correspondences. We conduct a comparative analysis of the registration accuracies achieved using the above methods and those obtained from traditional registration methods, including the Iterative Closest Point (ICP) algorithm. Target-based registration results serve as a benchmark for this analysis. Additionally, we study the impact of the various registration approaches on the estimated deformations and compare the TLS-based results to those obtained from plumb line measurements within the dam. The presented investigation uses real measurements from the Santa Maria dam in the Swiss Alps, but the findings are transferable to other geomonitoring application cases in non-urban environments.

Keywords: Terrestrial laser scanning (TLS), deformation analysis, point cloud registration, structural health monitoring, 3D vector fields

1 Introduction

Switzerland possesses approximately 150 hydroelectric dams, 80 % of which are located in the mountainous region of the country (Hauenstein and Lafitte, 2012). Governmental regulations require the owners of these structures to establish regular monitoring (Adam et al., 2023). Traditional solutions, such as geodetic networks, leveling, strain gauges, or plumb lines, coupled with manual inspections for cracks, have been in place for a long time (Kalinina et al., 2016). While providing highly accurate (up to sub-mm) and reliable point-wise data, these technologies lack the possibility of supplying areal data over the entire structure. Terrestrial laser scanning (TLS) offers an opportunity to bridge this gap.

Point cloud data need to be captured at different points in time (epochs) and be transformed into a common reference coordinate system before the actual deformation analysis. This registration process can either be accomplished by i) placing artificial targets in the scan scene and identifying them as corresponding points within the scans or ii) estimating correspondences directly from the scan data (cloud-based approaches). It is unclear which registration accuracies can be achieved in an alpine monitoring setting with either of these two general approaches.

The Iterative Closest Point (ICP) algorithm proposed by Besl and McKay (1992) is an established instance of the cloud-based approach. ICP recursively forms point correspondences between point clouds by nearest neighbor search in Euclidean space and iteratively refines the alignment by minimizing a distance metric. However, due to its simplicity in establishing correspondences, ICP is susceptible to the problem of local minima. Thus, it requires sufficiently accurate initialization. In addition, traditional ICP has no mechanism, other than maximum distance thresholding, to reject correspondences from non-stable areas in the context of registering scans from different epochs. Especially in the mountainous terrain of Swiss hydroelectric dams, where the surroundings are mostly comprised of jagged rock, loose debris, and highly irregular and repetitive surfaces due to vegetation, a robust correspondence search paired with an adequate (in)stability assessment is necessary.

The topic of establishing robust correspondences between point clouds is not only a fundamental problem in registration but also in monitoring and deformation estimation. For most point cloud–based deformation estimation algorithms, it is assumed that the point clouds are pre-aligned, and therefore, that the resulting (3D) vector fields represent true deformations. By removing this assumption and applying these algorithms to non-aligned point clouds, the interpretation of the resulting vector fields changes to a mixture of two signals: the pending registration and the true deformations. Hence, these deformation estimation algorithms could be leveraged for registration when combined with a strategy to separate these signals. Two examples of algorithms that could be used in combination with such a strategy are the Feature to Feature Supervoxel-based Spatial Smoothing (F2S3) method proposed by Gojcic et al. (2021), typically used for landslide monitoring, and our own Intensity Image Optical Flow for 3D displacements (IOF3D) method under development (Sec. 2). The degree to which such methods can be successfully leveraged for registration purposes is not yet clear.

Herein, we aim to investigate whether and how sufficient registration accuracy can be achieved for the specific use case of monitoring hydroelectric dams in mountainous terrain. We compare four different registration approaches, two established ones, and two experimental ones, adopted from deformation monitoring: Target-based registration, ICP, F2S3-based, and IOF3D-based registration. Their performance is evaluated using real monitoring data from the Santa Maria hydroelectric dam. The data were collected in collaboration with the owner of the dam (Kraftwerke Vorderrhein AG) and the surveying team of Axpo Power AG. The investigated registration methods are briefly described in Section 2, and the datasets in Section 3. We discuss the results (Sec. 4) in Section 5, and conclude in Section 6.

2 Methods

For all four investigated registration methods, we first perform a coarse registration of the secondary scans to the reference scan. We achieve this by computing each point's Fast Point Feature Histograms (FPFH) descriptor (Rusu et al., 2009). This pose-invariant descriptor describes the local geometry of each point based on a fixed number of neighboring points. Given the FPFH descriptors, we apply a Random Sample Consensus (RANSAC) approach (Fischler and Bolles, 1981) by repeatedly estimating the transformation parameters based on three randomly selected points in the secondary scan and their nearest neighbors in the reference scan within the feature space and evaluating the overall fit. Due to computational considerations and to equalize the neighborhood sizes for the FPFH calculation, the point clouds are spatially down-sampled for this coarse registration process. We use the full resolution point clouds unless stated otherwise for the following fine registration with the investigated methods. The methods and relevant implementation details are briefly presented in the following text.

Target-based: For the target-based approach, we estimate target center coordinates of black and white planar targets in each scan using the image correlation approach proposed by Janßen et al. (2019). This approach uses a combination of plane fitting and template matching of an idealized artificial target against the intensity images generated from the point clouds. Given a set of target center coordinates for each point cloud, we calculate the parameters to transform the secondary scans' coordinate systems to the project reference coordinate system given by the reference scan with a robust 7-parameter Helmert transformation. We include the scale estimation to compensate for changes in atmospheric conditions between the different scans. We separate outliers from inliers by performing RANSAC prior to the final estimation of the transformation parameters.

ICP: For our ICP analysis we use traditional ICP

(Besl and McKay, 1992) with a point-to-point objective function:

$$E(\mathbf{T}) = \sum_{(\mathbf{p},\mathbf{q})\in\kappa} ||\mathbf{p} - \mathbf{T}\mathbf{q}||^2 \tag{1}$$

where κ represents the set of correspondences by assigning to each point $\mathbf{q}$ in the source point cloud its nearest neighbor in Euclidean space $\mathbf{p}$ from the target point cloud. We use a multi-scale coarse-to-fine scheme for computational considerations to limit the number of iterations performed at full resolution (Jost and Hugli, 2002).

F2S3: F2S3 combines a feature-based correspondence search with a neural network-based outlier detection step. For this, the Distinctive 3D Local Deep Descriptor proposed by Poiesi and Boscaini (2021) is calculated for each point of the two point clouds. A nearest neighbor search within the feature space is then performed for each point in the source point cloud to find its corresponding point within the target point cloud. Due to computational considerations, the Hierarchical Navigable Small World Graphs method (Malkov and Yashunin, 2020) is used for an approximate nearest-neighbor search. For outlier removal, a local rigidity assumption is introduced by applying the supervoxel segmentation algorithm proposed by Lin et al. (2018) to the source point cloud and evaluating if, per supervoxel, a majority of correspondence vectors match a rigid body transformation.

IOF3D: The Intensity Image Optical Flow for 3D Displacements (IOF3D) detects displacements between two point clouds by leveraging well-established optical flow approaches. The point clouds are first converted into a set of range and intensity images, then 2D flow vectors are estimated between pairs of epochs using the Recurrent All-Pairs Field Transformers for Optical Flow algorithm (Teed and Deng, 2020). 3D displacements are then estimated with these 2D flow vectors and the range image information. A more in-depth publication on IOF3D is in the making at the time of writing this paper.

For both the F2S3- and the IOF3D-based approach, we first estimate the dense 3D vector fields with the given framework. We introduce the assumption that a majority of areas within the scan scene are stable between the two scans. This allows us to separate the registration and the estimation of deformations using a RANSAC-based transformation approach. Post RANSAC, we perform a final 7-parameter Helmert estimation with all the correspondences classified as inliers. This step mitigates the impact of quantization errors introduced during the initial vector field estimation. Such errors occur because both F2S3 and IOF3D require some form of discretization: F2S3 in the form of voxel-downsampling prior to the calculation of the point descriptors, and IOF3D through the 2D rasterization introduced by the conversion to intensity and range images.

Further implementation details are omitted for brevity, and the analysis of the impact of different (hyper-)parameters, e.g. the ones necessary for the mentioned discretization, is out of the scope of this study. We chose the parameters with care based on trial and error and prior experiences. The implemented workflows for coarse, ICP-based, and F2S3-based registration are based on open-source code (Open3D Python library and gseg-ethz GitHub repository). The code for the IOF3D-based registration workflow and overall performance analysis will be published in conjunction with the previously mentioned forthcoming publication.

3 Data set

3.1 Santa Maria hydroelectric dam

The Santa Maria hydroelectric dam is an arch dam located in the Swiss Alps. It measures 117 m in height and has a length of 560 m along the top of the dam. The dam contains six galleries along the entire length, of which three are monitored by geodetic measurements. In addition, a system of distributed automated plumb line measurements (Huggenberger AG Telelot VDD2V4) continuously monitors horizontal displacements with an accuracy of 0.05 mm at 13 positions in the dam structure.

We selected a spot on the small valley-side access road roughly 200 m from the foot of the dam as the scanner location. In combination with a heavy-duty tripod, this position offers enough ground stability in the otherwise rather marshy terrain while still being roughly equidistant to most of the dam's valley-side surface. Eight mounting points for the laser scan targets were permanently affixed to the rock face and large boulders in the vicinity of the scanner's selected position. The mounting points were

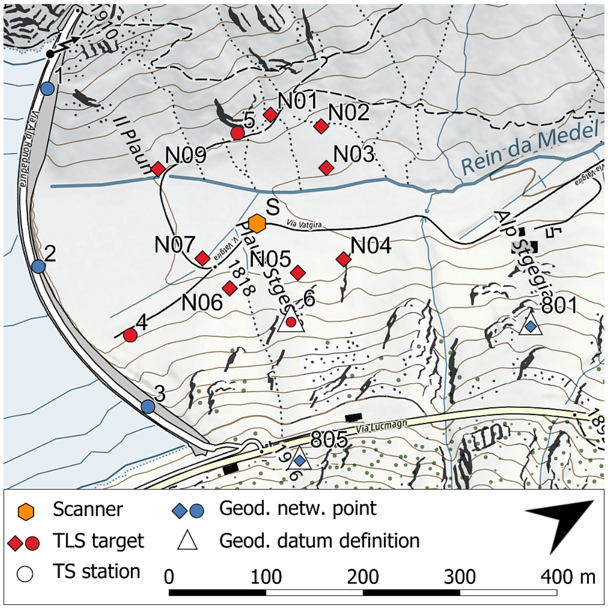

Figure 1. Overview map of the study site with positional markers for the scanner, black and white targets, geodetic network targets and stations, and geodetic datum definition.

positioned to achieve a roughly uniform distribution in all directions around the scanner location. The distances were mainly dictated by the availability of suitable surfaces and ended up being between 65 m and 120 m (Fig. 1). In addition, three pillars of the larger geodetic network used to control the stability of the dam were also included by placing 30×30 cm black and white targets on them (distance to the scanner between 95 m and 175 m). For both the rock- and pillar-based targets, mounting solutions were used that allowed for interchangeability with standard geodetic prisms. This enables control of the stability of the target coordinates over time using traditional geodetic network measurements.

3.2 Measurement campaigns

Two measurement campaigns were carried out in 2024 to capture the deformation of the dam between low (May) and high water (September) levels. During the first campaign, we collected TLS data with several repeated scans throughout one morning. For the second campaign, we collected data (nearly) continuously over two consecutive nights. For both campaigns, we used a Leica ScanStation P50 with the scan settings listed in Table 1. The manufacturer states the accuracies in this case as 3 mm + 10 ppm for the range measurements and $8''$ for the angular readings. By variance propagation, this results in an approximate 3D positional accuracy (Helmert point error) of 12 mm per point when taking into account the distance to the dam. Throughout both campaigns, meteorological parameters—air temperature, barometric pressure, and relative humidity—were recorded using a Reinhardt MWS 9-5 weather station positioned on a geodetic tripod a few meters from the scanner. Geodetic network measurements were carried out within each measurement campaign to ensure the stability of the target mounting points between the two epochs.

Table 1. Leica ScanStation P50 settings.

Parameter	Value
Resolution	1.6 mm@10 m
Field of view	Full dome scan
EDM mode	max distance 570 m
EDM sensitivity	Normal
Scan duration	54 min
Atmospheric settings	Standard atmosphere

3.3 Scan selection

For this investigation, we selected several scans from the entire acquisition, one reference scan and three secondary scans. This selection allowed us to investigate three scenarios: comparison between two scans i) *Same day*: collected one right after the other; ii) *Other day*: collected within the same campaign but with a longer time gap (approximately 22 hours) and with repositioning of the scanner setup (approx. 5 m away from the original); iii) *Other epoch*: from different measurement campaigns, i.e., approximately four months apart. We reduced the impact of atmospheric effects by choosing the four scans that had minimal changes in the refractive index of the atmosphere in proximity to the scanner during their individual acquisition times based on the meteorological data collected with the weather station, following the recommendations outlined by Friedli (2020, p. 83).

3.4 Reference data set

Plumb measurement data from eight locations within the dam are available for both measurement campaigns. The comparison of these data shows a deformation of the dam's top-center region between May and September of up to 2.5 cm radially in the direction of the valley (direction approximately in line with the surface normal of the dam). This deformation is expected and corresponds to the changes in water level and temperature. The measured deformations within each measurement campaign are negligible for this investigation (below 0.3 mm).

4 Results

We perform the scan registration for the three scenarios with each of the four methods described in Section 2. This results in twelve distinct registration solutions. Since the dam is the subject of deformation monitoring, and we thus assume it to deform, we remove it from the scans during registration. In addition, we remove all points below 15 m distance to the scanner to avoid impacting registration by geometrical changes in the scanner's proximity due to the modifications in the experimental setup (weather station, fuel cell, etc.). For all registration methods, we evaluate the registration quality based on the target coordinate residuals between the reference and secondary scans post-registration.

Additionally, to contextualize the impact of remaining registration errors on the use-case of hydroelectric dam monitoring, we estimate the deformation of the dam w.r.t. the surface normal using the Multiscale Model to Model Cloud Comparison algorithm (M3C2) introduced by Lague et al. (2013). M3C2 is suited for this purpose because the surface normal vectors align closely with the typically expected radial deformations of arch dams. For the scenarios *Same day* and *Other day*, we interpret any visible deformation in the M3C2 results to be false deformations, whereas for scenario *Other epoch*, we compare the M3C2 results to the available plumb line data. For this, we extract a 2×2 m patch at each plumb line measurement location from the M3C2 results and compute the averages within each patch.

4.1 Target coordinate residuals

The average target coordinate residuals w.r.t. the reference epoch are summarized for all approaches in Table 2. We can see that the target-based approach reliably results in average 3D residuals below 5 mm. For the target-based approach, scenario *Other epoch* displays a higher average 3D residual compared to *Same day* and *Other day*. A closer inspection of the robust Helmert transformation shows that two of the eleven targets (target 4 and N09) were marked as outliers. If we exclude the residuals from these two targets, the average 3D residual drops to 3.3 mm. Target 4 was also marked as an outlier in the robust Helmert transformation of scenario *Other day*. After exclusion, the average 3D residual is 2.2 mm. Target 4 has the largest distance of 175 m relative to the scanner.

Table 2. Post-registration target coordinate residuals w.r.t. target coordinates of the reference scan.

Method	**Scenario**	**Average target coordinate residuals (1σ in brackets)**			
		ΔX **[mm]**	ΔY **[mm]**	ΔZ **[mm]**	$\Delta 3D$ **[mm]**
Target-based	Same day	0.0 (1.7)	0.0 (1.6)	0.0 (1.2)	2.1 (1.6)
	Other day	-0.5 (2.1)	0.4 (1.3)	0.4 (2.7)	2.9 (2.3)
	Other epoch	0.0 (2.4)	-1.4 (3.4)	1.1 (2.7)	4.5 (2.8)
ICP	Same day	-17.6 (2.8)	-8.1 (1.5)	-0.9 (3.9)	19.9 (2.5)
	Other day	2.5 (2.1)	-4.6 (1.3)	2.3 (2.3)	6.5 (1.2)
	Other epoch	0.0 (7.5)	-20.0 (6.8)	-52.6 (5.4)	57.1 (6.7)
F2S3-based	Same day	15.9 (2.6)	-13.5 (1.4)	-3.2 (4.8)	21.7 (2.6)
	Other day	-0.7 (6.6)	9.0 (6.7)	-8.9 (3.7)	15.4 (5.0)
	Other epoch	10.3 (9.3)	-1.9 (7.8)	-33.7 (2.3)	37.2 (3.2)
IOF3D-based	Same day	4.2 (2.6)	8.3 (1.3)	1.7 (6.5)	11.5 (2.9)
	Other day	-6.4 (5.0)	-3.1 (2.5)	0.6 (10.3)	12.2 (6.4)
	Other epoch	-32.5 (10.4)	-6.7 (12.5)	-32.9 (25.2)	53.7 (14.4)

All non-target-based approaches show average 3D residuals that are worse by a factor of 2 to 10 compared to the target-based approach, with the scenario *Other epoch* being consistently the worst performing for each approach. While the IOF3D-based approach has similar results in the scenarios within an epoch, the results of both the ICP and the F2S3-based approaches show no such consistency. A

Table 3. Errors calculated from M3C2 deformation results for each of the investigated methods and scenarios.

Method	Median error [mm] (5th to 95th percentile spread in brackets)		Mean error [mm] (total spread in brackets)
	Same day	Other day	Other Epoch
Target-based	-0.5 (2.8)	1.8 (2.9)	-2.4 (5.3)
ICP	-14.2 (10.0)	0.2 (6.1)	-12.3 (33.9)
F2S3-based	-0.7 (17.7)	-7.8 (11.6)	13.3 (18.8)
IOF3D-based	4.1 (10.9)	-7.4 (8.4)	15.7 (17.0)

closer inspection of the individual coordinate component residuals shows that while the Z-components have similar or better residuals for the scenarios *Same day* and *Other day* compared to the other two components, they (Z-component residuals) are the highest in the *Other epoch* scenario.

4.2 Dam deformation

The results of the M3C2 deformation estimation are summarized in Table 3 for all registration approaches. We use two metrics to evaluate the registration quality and its impact on the subsequent deformation analysis: bias and spread. For the scenarios *Same day* and *Other day*, we use the median as a robust bias estimator and the difference between the 5th and 95th percentile as a robust metric of spread, calculated directly from the approximate 2.2 million M3C2 estimates covering the entire visible dam surface (plumb line measurements indicate negligible deformations for these scenarios). For the scenario *Other epoch*, we first compute the difference between the plumb line measurements and the average M3C2 results of the corresponding 2×2 m patch. Due to the insufficient number of data points for a robust analysis (only eight available plumb line measurement positions within the field of view), we use the mean as an indicator of the bias, and the span as an indicator of the spread. The target-based approach leads to a consistent spread of around 3 mm for the first two scenarios, with scenario *Same day* having an almost unperceivable bias and scenario *Other day* displaying a bias below 2 mm. Additional inspection of a visual representation of these results shows the presence of a vertical stripe pattern (Fig. 2). These stripes are most pronounced towards the left and right edges of the dam structure and can exhibit deviations of up to ± 4 mm from the bias, therefore exceeding the calculated spread.

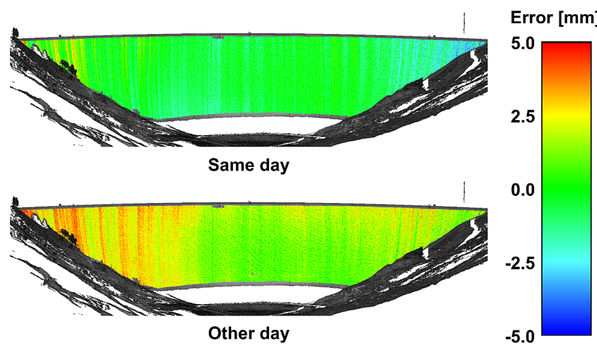

Figure 2. Visualization of the M3C2 analysis for scenarios *Same day* (top) and *Other day* (bottom) following the target-based registration method.

We observe that the target-based approach outperforms the other ones up to one order of magnitude when taking both bias and spread into account, as was already indicated by the target coordinate residuals. Similarly to the previous results, all non-target-based methods perform equally poorly. Independent of the registration method, the *Other epoch* scenario has the highest spread among all scenarios. We show the effects of high bias with low spread, and vice versa, by two representative results in Figure 3.

5 Discussion

While the analysis of target center coordinate residuals using the target-based registration method showed very similar performance for the *Same day* and *Other day* scenarios, the M3C2 analysis, which is an integral part of the chosen monitoring strategy, revealed a bias in the second scenario. This demonstrates the need for an analysis of registration errors on the use-case of the specific project. Conversely, interpreting solely the M3C2 analysis re-

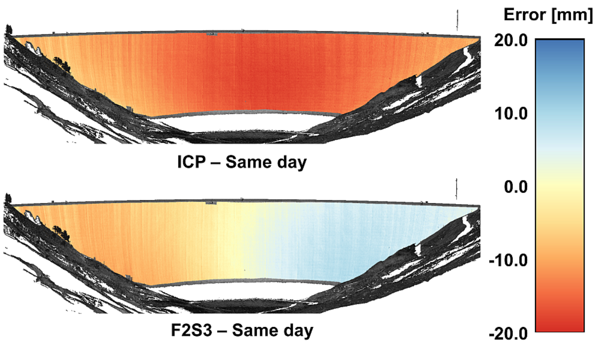

Figure 3. Representative visualization of high bias (top) and high spread (bottom).

sults would indicate smaller registration errors than estimated from the target residuals. Especially, the errors in the Z-component are masked by the M3C2 estimation of the arch dam structure. This highlights the need for a target-based ground truth analysis for more generalized investigations of registration algorithms, beyond specific use-cases.

Furthermore, we observed a clear decrease in performance between scenarios *Same day*/*Other day* and *Other epoch*. While for the target-based approach, our results indicate that this equates to an increase in uncertainty of only a few mm, the results of the non-target-based methods show a decrease in performance on the level of multiple cm. This indicates that not only ICP, but also the two experimental methods, F2S3-based and IOF3D-based, which are designed to separate true deformation signals from registration information, struggle with changes in the environment between epochs. The increase in the Z-component residuals points towards the change in vegetation between May and September as a possible error source contributing to the degradation of non-target-based registration between the epochs.

Systematics in the form of vertical stripes with increasing error magnitudes up to 4 mm towards the edges are visible throughout the M3C2 results. The pattern, coupled with the increase in the angle of incidence of up to 30° towards the edges of the dam and the vicinity of the line of sight to the valley flanks, could indicate both a connection to beam bending due to atmospheric refraction and (colored) noise in the readings of the instrument's angular encoders.

In general, we observe an approximate order of magnitude difference between the performance of the target-based and the non-target-based approaches. This indicates that the investigated non-target-based approaches struggle to various degrees with establishing correct correspondences for registration in this mountainous scene, regardless of whether changes are present or not. The residuals and M3C2 evaluation of the target-based registration approach are in line with the manufacturer-stated accuracies of the instrument used in this study, indicating that the inaccuracy introduced by the registration approach itself is not the dominating source of error but rather a combined effect with other inherent error sources, such as refraction, calibration or general instrumental errors, etc. Hence, for further accuracy gains, if required, other effects need to be addressed as well. This is in contrast to the non-target-based methods, where the registration errors are significantly higher. Instead, these methods introduce dominating sources of inaccuracy that require further investigation to identify and mitigate.

6 Conclusion & Outlook

In this study, we showed that a target-based registration can be used to facilitate reliable deformation estimates of a hydroelectric dam with an uncertainty of below 5 mm. These values are derived by comparing the estimation results to ground truth data obtained by plumb line measurements. We further compared these results to the established cloud-based registration approach (ICP) and newer approaches that leverage more sophisticated point correspondence establishment techniques. The comparison showed that all non-target-based approaches perform up to an order of magnitude worse than the target-based approach in this large-scale, non-urban environment. Particularly in combination with changes in the registration scene between epochs, these algorithms struggle to produce reliable correspondences of only stable areas, which are needed to estimate registration parameters at an accuracy level comparable to the target-based approach. Future work is required to develop methods that reliably identify stable areas and select correspondences accordingly.

Acknowledgments

We would like to thank Kraftwerke Vorderrhein AG for their financial and logistical support, and for granting us access to the dam. We would also like to thank Annelies Voordendag for her support during the measurement campaigns, as well as Robert Presl and Thomas Posur for their efforts in preparing the instrumentation for the fieldwork.

Disclaimer

We used AI tools—ChatGPT 4o and Grammarly—to assist with the initial language editing and for coding (Python). We take full responsibility for this paper's content, language, and appearance.

References

Adam, N. J., Filliez, J., and Fauriel, J. (2023). Ageing dams in Switzerland: Feedbacks of several case studies. In *Role of Dams and Reservoirs in a Successful Energy Transition*, pages 613–621. CRC Press.

Besl, P. and McKay, N. D. (1992). A method for registration of 3-D shapes. *IEEE Transactions on Pattern Analysis and Machine Intelligence*, 14(2):239–256.

Fischler, M. A. and Bolles, R. C. (1981). Random Sample Consensus: A paradigm for model fitting with applications to image analysis and automated cartography. *Commun. ACM*, 24(6):381–395.

Friedli, E. (2020). *Point Cloud Registration and Mitigation of Refraction Effects for Geomonitoring Using Long-Range Terrestrial Laser Scanning*. Doctoral Thesis, ETH Zurich, Zurich, Switzerland.

Gojcic, Z., Schmid, L., and Wieser, A. (2021). Dense 3D displacement vector fields for point cloud-based landslide monitoring. *Landslides*, 18:3821–3832.

Hauenstein, W. and Lafitte, R. (2012). Impacts of dams in Switzerland. In Tortajada, C., Altinbilek, D., and Biswas, A. K., editors, *Impacts of Large Dams: A Global Assessment*, pages 95–122. Springer Berlin Heidelberg, Berlin, Heidelberg.

Janßen, J., Medic, T., Kuhlmann, H., and Holst, C. (2019). Decreasing the uncertainty of the target center estimation at terrestrial laser scanning by choosing the best algorithm and by improving the target design. *Remote Sensing*, 11(7).

Jost, T. and Hugli, H. (2002). A multi-resolution scheme ICP algorithm for fast shape registration. In *Proceedings. First International Symposium on 3D Data Processing Visualization and Transmission*, pages 540–543.

Kalinina, A., Spada, M., Marelli, S., Burgherr, P., and Sudret, B. (2016). Uncertainties in the risk assessment of hydropower dams: state-of-the-art and outlook. Research report, Paul Scherrer Institute, 5232 Villigen, Switzerland; ETH Zurich, Chair of Risk, Safety and Uncertainty Quantification, Stefano-Franscini-Platz 5, 8093 Zurich, Switzerland.

Lague, D., Brodu, N., and Leroux, J. (2013). Accurate 3D comparison of complex topography with terrestrial laser scanner: Application to the Rangitikei canyon (N-Z). *ISPRS Journal of Photogrammetry and Remote Sensing*, 82:10–26.

Lin, Y., Wang, C., Zhai, D., Li, W., and Li, J. (2018). Toward better boundary preserved supervoxel segmentation for 3D point clouds. *ISPRS Journal of Photogrammetry and Remote Sensing*, 143:39–47.

Malkov, Y. A. and Yashunin, D. A. (2020). Efficient and robust approximate nearest neighbor search using hierarchical navigable small world graphs. *IEEE Transactions on Pattern Analysis and Machine Intelligence*, 42(4):824–836.

Poiesi, F. and Boscaini, D. (2021). Distinctive 3D local deep descriptors. In *IEEE Proc. of Int'l Conference on Pattern Recognition*, Milan, IT.

Rusu, R. B., Blodow, N., and Beetz, M. (2009). Fast point feature histograms (FPFH) for 3D registration. In *2009 IEEE International Conference on Robotics and Automation*, pages 3212–3217.

Teed, Z. and Deng, J. (2020). RAFT: Recurrent all-pairs field transforms for optical flow. In Vedaldi, A., Bischof, H., Brox, T., and Frahm, J.-M., editors, *Computer Vision – ECCV 2020*, pages 402–419, Cham. Springer International Publishing.